### Title
Using Conditional Random Fields for a Spatially Variable Liquefiable Foundation Layer in Nonlinear Dynamic Analyses of Embankments




### Journal
Journal of Geotechnical and Geoenvironmental Engineering, 147(11)

### ISSN
1090-0241



### Authors
Paull, Nicholas A
Boulanger, Ross W
DeJong, Jason T
et al.



### Publication Date
2021-11-01

### DOI
10.1061/(asce)gt.1943-5606.0002610

Peer reviewed

# Using conditional random fields for a spatially variable liquefiable foundation layer in nonlinear dynamic analyses of embankments

By

Nicholas A. Paull, Ph.D., A.M.ASCE
*Corresponding Author: Project Engineer, GEI Consultants Inc.,*
*Rancho Cordova, CA 95670, npaull@geiconsultants.com*

Ross W. Boulanger, Ph.D., P.E., F.ASCE
*Professor, Department of Civil and Environmental Engineering,*
*University of California, Davis, CA 95616, rwboulanger@ucdavis.edu*

Jason T. DeJong, Ph.D., M.ASCE
*Professor, Department of Civil and Environmental Engineering,*
*University of California, Davis, CA 95616, jdejong@ucdavis.edu*

Steven J. Friesen, P.E.
*Senior Engineer, California Department of Water Resources*
*Sacramento, CA 95814, Steven.Friesen@water.ca.gov*

ASCE Journal of Geotechnical & Geoenvironmental Engineering (in press)
Authors' final copy
2021

**Abstract**

Two-dimensional nonlinear dynamic analyses (NDAs) are performed for a series of hypothetical embankment dams on a spatially variable liquefiable foundation layer to evaluate the utility of representing the foundation layer with random fields conditioned on different levels of site characterization information. A set of two-dimensional parent models (PMs), each representing a "true" foundation condition, were generated using unconditional random fields of equivalent clean sand, corrected Standard Penetration Test $(N_1)_{60cs}$ values. Different levels of site characterization were then represented by combining different numbers of "local borings" (i.e., columns of data from the parent model) with the optional inclusion of constraints on the geostatistical properties that might come from "site-wide explorations." NDAs were performed using the same input motions for the parent model (which represents perfect knowledge of soil conditions), a set of realizations conditioned on the local borings alone, and a set of realizations conditioned on the local borings with site-wide statistics. Embankment deformations obtained for the conditional realizations are compared to those for the parent model to evaluate the potential benefits of increasing levels of site characterization in terms of deformation prediction accuracy. Parametric analyses include varying the embankment size, scales of fluctuation in the foundation stratum, number of conditioning borings, and ground motions. The results of these comparisons illustrate that beneficial effects of using conditional random fields were generally limited to cases with the horizontal scale of fluctuation approaching the scale of the embankment base width and to cases with a large number of borings (greater than three borings per horizontal scale of fluctuation) which may not be practical in many situations. Additional potential benefits and limitations of using conditional random fields for representing spatial variable liquefiable foundation layers in embankment dam NDAs are discussed.

**Introduction**

Consideration of spatial variability in soil properties has been accounted for using random fields for many different geotechnical systems including foundations, dams and slopes. In most of these studies, unconditional random fields are used to represent situations in which site investigations are used to inform selection of random field properties (e.g., mean, coefficient of variation, scales of fluctuation), but are not directly incorporated in the random fields as is done with conditional random fields. Joint TC205/TC304 Working Group (2017) summarized thirteen studies that were conducted using primarily unconditional random fields to assess the stability of different geotechnical systems. These studies have generally concluded that the critical correlation length (the correlation length for which the range of deformations is the largest) is within a range of 0.5 to 2 times the base length of the geotechnical system (e.g., Fenton et al. 2005, Griffiths et al. 2006). Liu et al. (2017) completed a study that used conditional random fields for slope stability analyses wherein they summarized the contributions of an additional twenty studies using conditional and unconditional random fields of soil properties to assess static slope stability. The studies that used conditional random fields for slope stability analyses generally showed potential benefits in directly incorporating site investigation data into the random fields depending on the spacing between site investigation locations, scales of fluctuation, and the size of the geotechnical system. The greatest benefits from conditioning the models in many of these studies are for cases that had correlation lengths on a similar scale as their critical correlation lengths. None of these studies considered seismic deformations with the occurrence of strongly nonlinear soil behavior (e.g., liquefaction), which together may significantly impact the comparison of deformations between models with unconditional and conditional random fields. This study will assess whether the benefits of using conditional random fields in NDAs of embankments on liquefiable soils are similar to those observed in static stability analyses.

A few prior studies have utilized unconditional random fields in NDAs to assess potential seismic deformations of embankment dams. Boulanger and Montgomery (2016) conducted two-dimensional (2D) NDAs of a 45 m high embankment dam on uniform and stochastic realizations of Standard Penetration Test (SPT) $(N_1)_{60cs}$ values in an alluvial foundation layer. Paull et al. (2019) conducted 2D NDAs of 5 m to 45 m high embankment models, and concluded that the representative percentile for $(N_1)_{60cs}$ values increased with increasing normalized scale of fluctuation ($\theta_x$ /B, where $\theta_x$=horizontal scale of fluctuation and B=embankment base length) for the models with $\theta_x$ /B between 0 and 0.8. Both Montgomery and Boulanger (2016) and Paull et al. (2019) conclude that the 45$^{th}$ to 50$^{th}$ percentile $(N_1)_{60cs}$ could be used in a uniform model for an alluvial foundation stratum to estimate the median embankment deformations and that the 30$^{th}$ to

33rd percentile could be used in a uniform model for an alluvial foundation stratum to obtain reasonably conservative estimates of embankment deformations. Both studies acknowledged that their results could be impacted by the geometry of the structure and deformation mechanisms, variability of input motions, variability of soil properties, and quality of site explorations. These results are consistent with those for other geotechnical systems (e.g., Baecher and Ingra 1981, Fenton and Griffiths 2008, Joint TC205/TC304 Working Group 2017) that showed there was a critical correlation length of approximately 0.5B to 2B where stochastic models produce the largest standard deviation of deformations. Paull et al. (2020) presented preliminary results from embankment models with conditional realizations of alluvial $(N_1)_{60cs}$ (hereafter referred to as conditional models) to embankment models with the same geometries but with unconditional realizations of alluvial $(N_1)_{60cs}$ (hereafter referred to as unconditional models). That study found that the benefits of conditioning the random fields to SPT data obtained on site could be limited by: (1) the lack of site investigation data in locations critical to the deformation mechanisms, and (2) the distributions of the measured SPT $(N_1)_{60cs}$ being different than the true distribution of the in situ $(N_1)_{60cs}$. In addition, the total uncertainty in estimated deformations includes contributions from several sources (soil properties, earthquake motions, numerical model, reservoir level, etc.), which will limit the overall reduction in deformation uncertainty that can be obtained using conditional realizations.

The current study uses 2D NDAs of hypothetical embankment dams on a spatially variable liquefiable foundation layer to evaluate the utility of representing the foundation layer with random fields conditioned on different levels of site characterization information. A set of two-dimensional parent models, each representing a "true" foundation condition, were generated using unconditional random fields of equivalent clean sand, corrected Standard Penetration Test $(N_1)_{60cs}$ values. Different levels of site characterization were then represented by combining different numbers of "local borings" (i.e., columns of data from the parent model) with the optional inclusion of constraints on the geostatistical properties that might come from "site-wide explorations." NDAs were performed using the same input motions for the parent model (which represents perfect knowledge of soil conditions), a set of realizations conditioned on the local borings alone, and a set of realizations conditioned on the local borings and site-wide statistics. Embankment deformations obtained for the conditional realizations were compared to those for the parent model to evaluate how increasing levels of site characterization might improve the accuracy of deformation predictions. These numerical comparisons of "true conditions" and conditional realizations maintain all other analysis parameters and constraints equal so that the differences in deformations are attributable to the stratigraphic differences in the conditional realizations. The deformations obtained in any one NDA are dependent on the system geometry, input parameters, ground motions, and modeling assumptions (geostatistical, constitutive, and numerical), and thus the relative differences in deformations for the true and conditional cases may also be dependent on these same factors, although presumably to a significantly lesser degree. Parametric analyses included varying the embankment size, scales of fluctuation in the foundation stratum, number of conditioning borings, and ground motions. The results of these parametric analyses are used to illustrate potential benefits and limitations in using conditional random fields for representing spatial variable liquefiable foundation layers in NDAs for levees or embankment dams, while recognizing that the actual benefits will depend on specific site and loading conditions.

**NDA embankment models**

The two-dimensional NDAs for this study represent numerical experiments designed to isolate and evaluate the relative utility of representing the foundation layer with random fields conditioned on different levels of site characterization information. The key assumption is that factors that impact results from an NDA model with an unconditional random field representing the $(N_1)_{60cs}$ values in the foundation alluvium will have approximately equal impacts on results from an NDA model with all other aspects the same except for the conditioning of the random field. At the same time, it is unlikely that any quantitative evaluation of potential reductions in bias or dispersion through the use of conditional realizations can be generalized for application in practice, as the dispersion in deformations is itself significantly affected by the nature and distributions of properties in the embankment and foundation and the nature of the loading. The number of realizations and ground motions presented in the following sections are therefore considered sufficient, for comparative purposes, to qualitatively identify whether there was a marked reduction in the variability of calculated deformations.

***Model configuration***

Embankments with heights of 45 m, 25 m and 10 m, as shown in Figure 1, are analyzed using the 2D finite difference program FLAC 8.0 (Itasca 2016). The embankments have the same overall geometry and properties as presented in Paull et al. (2019, 2020) including the same embankment slopes (2.5H:1V for the shells and 3.5H:1V for the downstream berm) and the same material groups (bedrock, alluvium, clay core and embankment shells). The alluvium is represented with random fields of $(N_1)_{60cs}$ values, as described later, whereas other material groups are modeled with uniform properties.

Embankment model stresses are initialized through an incremental process to simulate conditions that occur during construction and checked to ensure reasonable conditions prior to dynamic loading. Embankment models are created in increments that are a single element high to simulate construction and the upstream water level is increased in five levels to a final water level of 75% of the embankment height to simulate reservoir filling. All stress conditions are checked based on the recommendations in Boulanger and Beaty (2016) to ensure reasonable stress and seepage conditions at the time of shaking.

***Material properties and model calibration***

The material properties and calibrations for the four material groups are presented in Paull et al. (2019, 2020) and briefly summarized herein.

The elastic bedrock is modeled with a permeability, k=5.0E-6 cm/s, a shear modulus, G=1800 MPa, Poisson's ratio, $\nu$=0.3, and saturated unit weight, $\rho$=2.2 Mg/m$^3$, which together correspond approximately to a shear wave velocity $V_s$=905 m/s.

The clay core is modeled as a Mohr-Coulomb material with anisotropically consolidated undrained (ACU) shear strengths computed using the procedures in Duncan and Wright (2005) as applied to NDA models by Montgomery et al. (2014). The ACU shear strengths are calculated using undrained shear strength parameters for isotropic consolidation; $d_R$=33 kPa and $\psi_R$=14°, and the drained shear strength parameters; $d_S$=c'=0 and $\psi_S$=$\phi$'=36°. The shear modulus is set proportional to the square root of the mean effective stress (p'), with G= 43 MPa at p'=101.3 kPa. The permeability and saturated unit weight of the core is 5.0E-5 cm/s and ρ=2.0 Mg/m$^3$ respectively.

The shell and alluvium materials are modeled using PM4Sand version 3.1 (Boulanger and Ziotopoulou 2017) with the properties for each individual zone based on its assigned SPT $(N_1)_{60cs}$ value. SPT $(N_1)_{60cs}$ values are 35 for the shells and are Gaussian random fields for the alluvium (as described in the next section). The relative density ($D_R$) and shear modulus coefficient ($G_o$) are calculated based on the correlations to SPT $(N_1)_{60cs}$ used in Boulanger and Ziotopoulou (2018) with the contraction rate parameter ($h_{po}$) calibrated based on single-element direct simple shear simulations to match the cyclic resistance ratio (CRR) at an effective overburden stress of 1 atm (101 kPa) based on the SPT based liquefaction triggering correlation from Boulanger and Idriss (2012). Values of $h_{po}$ were calibrated for $(N_1)_{60cs}$ between 1 and 35 in increments of 1 and stored in a look-up table. Values of $h_{po}$ for individual zones in the NDA model were linearly interpolated from the look-up table based on its $(N_1)_{60cs}$ values. The remaining PM4Sand input parameters were kept at the default values. These calibrations produce cyclic resistances that decrease with increasing overburden stress and vary with initial static shear stresses, by amounts that depend on the overburden stress and $(N_1)_{60cs}$ value as described in Ziotopoulou and Boulanger (2016). The permeability of the alluvium and shells is 5.0E-4 cm/s and the saturated unit weights are 2.0 Mg/m$^3$ and 2.1 Mg/m$^3$ respectively.

***Representation of the alluvium***

A set of seven parent models, each representing a "true" foundation condition, were generated using unconditional random fields of $(N_1)_{60cs}$ values. The Gaussian random fields were defined with a mean $(N_1)_{60cs}$ of 15, a coefficient of variation, COV, of 0.4, and are truncated at a minimum $(N_1)_{60cs}$ value of 1.0 which affected less than 0.5% of the alluvial zones. Scales of fluctuation, or the distance within which points are significantly correlated (Fenton and Griffiths 2008), as mathematically defined in Vanmarcke (2010) were selected to be 1m in the vertical direction, $\theta_y$, and 10 m, 20 m or 60 m in the horizontal direction, $\theta_x$ depending on the analysis case. These COV values and scales of fluctuation are consistent with typical ranges reported in Phoon and Kulhawy (1999), while recognizing that spatial variability in many depositional environments may be far more complex and scale-dependent than a Gaussian random field can accurately represent. Despite their limitations in practice, these idealizations provide a means for examining the effects of different parameters under a manageable range of conditions.

Conditional random fields are created by using different numbers of "local borings" (i.e., columns of data from the parent model) with the optional inclusion of constraints on the geostatistical properties that might come from "site-wide explorations." The number of borings ranged from one to ten borings, depending on the analysis case, with the boring locations located primarily beneath the downstream shell for cases with a lower number of borings due to practical considerations involved in site investigation of most embankment dams. Boring locations are shown in Figure 1 for the 10 m, 25 m and 45 m tall embankments with 3 borings, and in Figure 2 for the 10 m embankment cases with various number of borings. The site-wide statistics are defined as the mean, COV, and scales of fluctuation used to generate the parent model, and thus represent perfect knowledge of these parameters. For cases without knowledge of the site-wide statistics, the mean, COV and $\theta_y$ are instead derived from the local borings alone, whereas the exact $\theta_x$ is still used (i.e., assumed to be accurately estimated from geology). Conditional random fields are created from the local borings with and without the site-wide statistics using LU (lower-upper) decomposition of the covariance matrix (Davis 1987, as implemented by Constantine and Wang 2012). The conditional random fields are perfectly conditioned on the input borings with some minor rounding errors that do not significantly affect the deformations or the overall conclusions. For each scenario, seven realizations were generated for the case without site-wide statistics and seven realizations were generated for the case with site-wide statistics.

The nature of conditional realizations is illustrated in Figure 3 showing profiles of SPT $(N_1)_{60cs}$ values at five locations beneath a 10 m tall embankment. The black bullet symbols show the true $(N_1)_{60cs}$ values from the parent model. The color symbols are the $(N_1)_{60cs}$ values from three realizations that were conditioned on two local borings (the middle and right-most profiles in this figure) with site-wide statistics. The conditional realizations match the borings used for conditioning, but otherwise produce a wide variation in possible $(N_1)_{60cs}$ values throughout the foundation layer. This figure indicates that the two borings, placed approximately 27 m apart did not have a significant effect in conditioning the $(N_1)_{60cs}$ values at the other three locations for the conditional models with $\theta_x$ = 20 m. The variability in computed embankment deformations, as discussed later, reflect the differences in where the looser and denser zones in these realizations are located relative to the embankment.

***Analysis groups***

Thirteen analysis groups, as listed in Table 1, were created to cover a range of embankment sizes, horizontal scales of fluctuation, and number of borings. Each analysis group involved performing NDAs for 49 models for any given ground motion, as follows. First, analyses were performed for the seven unconditional parent models, each with their only difference being the realization of alluvial $(N_1)_{60cs}$, from which three were selected to represent the lower, middle, and upper range of embankment deformations. Therefore, unless a specific difference in statistical values in the alluvium are stated (e.g.; mean, COV or scales of fluctuation of the alluvial $(N_1)_{60cs}$), parent models with the same numbering have the same alluvial $(N_1)_{60cs}$ realization. For each of the three selected parent models, NDAs were performed for the seven realizations that were conditioned on local borings alone and the seven realizations that were conditioned on local borings with site-wide statistics, as depicted in Figure 4 for analysis group 1. Select analysis groups were repeated with different input motions. Computation times on a multicore workstation ranged from 6 to 24 hours per simulation depending on the ground motion and other parameters.

***Input motions***

Embankment models are subjected to the TCU075 station east-west outcrop motion obtained from the NGA-West2 database (Ancheta et al. 2014), as recorded from the 1999 Chi-Chi earthquake (M=7.6) and scaled to a PGA of 0.6 g unless otherwise stated. The Mudurnu station fault normal (FN) motion from the 1999 Duzce earthquake (M=7.1), and the TAPS pump station number 10-047 recording from the 2002 Denali earthquake (M=7.9) each scaled to a PGA of 0.6 g are used on selected embankment models to compare the effects of different ground motions. These motions (see Figure 5) are chosen to represent a variety of spectral shapes, durations, fault slip mechanisms and locations.

Each ground motion is input as a shear stress time series to the compliant base of the embankment models based on the recommendations in Mejia and Dawson (2006). Free field conditions are applied to the lateral edges of each model. Alluvial zones connected to the lateral boundaries are modeled as elastic with a secant shear modulus equal to 70% of the small strain shear modulus computed for each zone's assigned $(N_1)_{60cs}$ value and confining stress to maintain lateral restraint for the adjacent PM4Sand elements. The post-shaking response, in which residual strengths were assigned using the procedures described in Paull et al. (2020), resulted in negligible additional deformations for the cases examined herein. A Rayleigh damping of 0.5% at a frequency of 3 Hz is applied to all materials to provide a minimum level of damping in the small strain range for nonlinear materials and a nominal damping for the elastic bedrock material.

**NDA Results**

NDAs were completed as undrained analyses with embankment deformations obtained at the end of strong shaking for all models. Embankment deformations obtained at the end of strong shaking for the conditional models were compared to those for the parent model to evaluate the potential improvements in deformation prediction accuracy with increasing levels of site characterization. Potential reductions in deformation uncertainty are evaluated by comparing sample standard deviations for the conditional models, with the standard deviations computed based on Johnson and Bhattacharyya (2010) given the small number of cases examined. Other measures of dynamic response can be important in certain situations, but embankment displacements are generally a primary concern in seismic evaluations. Displacements compared in these analyses include crest settlement and embankment stretch. Crest settlements are obtained as the vertical deformation of the embankment crest which is often used to assess the potential for cracking, loss of freeboard, or uncontrolled release of a reservoir. Embankment stretches are the increase in embankment base length ($\Delta B$) taken as the difference in the horizontal displacements of the embankment toes. Embankment stretch is preferred over using the displacements of the two toes separately, because stochastic realizations sometimes result in a large outward displacement at one toe or the other, and the statistics on embankment stretch (which reflects large displacements at either toe) are better behaved than the statistics for displacement at either toe alone. Crest settlements are normalized by the embankment height (H) and embankment stretch is normalized by the embankment base length (B).

***Impacts of embankment size***

Embankment deformations for analysis groups 1, 2, and 5, corresponding to embankment heights of 45 m, 25 m, and 10 m, respectively, with the TCU motion scaled to a PGA of 0.6 g are compared in Figure 6. Normalized crest settlements ($\Delta_{set}/H$) and their standard deviations are shown in Figures 6a and 6c, respectively. Normalized stretches ($\Delta_{str}/B$) and their standard deviations are shown in Figures 6b and 6d, respectively. The results are binned by embankment height, per the vertical separating lines on each figure and the labels at the bottom of Figures 6b and 6d. The red symbols show results for the seven unconditional realizations that were generated from the site-wide statistics alone. Three parent models were selected from these unconditional realizations; the parent models are identified by their realization number at the bottoms of Figures 6a and 6b. For each parent model, the single green symbol shows the deformation obtained for the parent model, the seven dark blue triangles show the results for the realizations conditioned on three local borings with site-wide statistics, and the seven cyan triangles show the results for the realizations conditioned on three local borings alone. The locations of the borings for each embankment height were shown previously in Figure 1.

The variability in normalized deformations for both the unconditional and conditional models increases with decreasing embankment height, which is consistent with expectations for the range of $\theta_x/B$ represented by these cases (Table 1). The 45 m tall embankment corresponds to $\theta_x/B = 0.08$, which means that the global deformation mechanisms are generally a few times larger than $\theta_x$. This results in greater averaging of material responses and less variability in deformations for a given input motion. The 10 m tall embankment corresponds to $\theta_x/B = 0.35$, which means that the global deformation mechanisms are similar in scale to $\theta_x$ which results in less averaging of material responses and greater variability in deformations. For all three embankment heights, the variability in deformations for the conditional models is comparable with or without the inclusion of site-wide statistics (i.e., blue versus cyan symbols). These two sets of conditional models give similar results because the three local borings proved to be sufficient to obtain reasonable consistent and accurate estimates of the mean $(N_1)_{60cs}$, COV, and $\theta_y$ values. The variability in deformations for both sets of conditional models is comparable to the variability in the unconditional models (red symbols) for the 10 m tall embankment, but appears to be slightly greater for the 45 m tall embankment. This apparent difference in variability for the 45 m tall embankment may be partly attributed to the relatively small number of unconditional realizations analyzed, but also appears partly due to the conditional models tending to produce slightly longer or more interconnected looser zones at the boring locations than actually existed in the parent models. Regardless, the results in Figure 6 do not show significant benefits from the use of conditional models over unconditional models, given that there were only three local borings and all three sets of models are based on the same or similar estimates of the stratum's geostatistical properties.

For the 45m tall embankment, the dispersion in deformations was not very large and therefore, the dispersion of deformations due to other sources of uncertainty (i.e., uncertainties in the input motions, soil properties, reservoir level, and numerical modeling procedures) would likely be more important in design. For this case there would be little motivation to do conditional realizations because they would not significantly reduce the total dispersion in calculated deformations. Therefore, further analyses focus on the smaller embankments where the dispersion in deformations was larger and could potentially be decreased by the use of conditional random fields.

***Impacts of scales of fluctuation***

Embankment deformations for analysis groups 5, 11 and 13, corresponding to a 10 m tall embankment on foundation layers with $\theta_x$ of 10 m, 20 m, and 60 m, respectively, with the TCU motion scaled to a PGA of 0.6 g are compared in Figure 7. These analysis groups represent $\theta_x/B$ of 0.17, 0.35, and 1.05 (Table 1) and used three borings (Figure 3c) for generating the conditional models. The deformations obtained from the conditional models, with or without use of site-wide statistics (blue and cyan symbols), are comparable in magnitude and variability to those obtained with the unconditional models (red symbols) for all three $\theta_x$. The $\Delta_{set}/H$ for the unconditional models ranged from about 5-17%, from which parent models (green symbols) were selected that had $\Delta_{set}/H$ of 6% (PM3), 13% (PM2), and 17% (PM7). The conditional models based on PM3 gave $\Delta_{set}/H$ of 6-12% (i.e., all greater than obtained with PM3 itself), whereas the conditional models based on PM7 gave $\Delta_{set}/H$ of 5-11% (i.e., all less than obtained with PM7 itself). The deformations for PM3 and PM7 were at the low and high end of those obtained from the unconditional realizations, respectively, because of where their larger zones of denser/looser materials tended to be located relative to the embankment. The conditional realizations generated from PM3 and PM7 do not recreate the same advantageous/disadvantageous spatial distributions because the three local borings are insufficient for accurately constraining the realizations. Instead, the conditional realizations tend to produce a range of realistic distributions that span from those existing in the parent model to those represented by the unconditional models. Overall, the results in Figure 7 do not show obvious benefits from the use of conditional models over unconditional models, given that there were only three local borings and all three sets of models are based on the same or similar estimates of the stratum's geostatistical properties.

Cases with horizontal scales of fluctuation greater than 60 m were not considered because at that scale, it becomes likely that several borings would encounter similar soil properties at similar elevations, which may then be represented in the geologic model as a distinct substratum for purposes of NDAs. For example, an extended zone of looser soil within an alluvial deposit may be interpreted as a separate subunit as was done for Perris Dam by URS (2012). This approach of representing larger zones of looser soils as subunits for purposes of assigning distinctive properties is common in practice.

***Impacts of the number of conditional borings***

Embankment deformations for analysis groups 5 through 9, corresponding to the foundation layer being characterized by 1, 2, 3, 5, or 10 borings, respectively, are compared in Figures 8 (for 1, 2, and 3 borings) and 9 (for 3, 5, and 10 borings). These analyses are for a 10 m tall embankment, a foundation $\theta_x$ = 20 m ($\theta_x$ /B = 0.35), and the TCU motion scaled to a PGA of 0.6 g. The different numbers of borings are located as shown in Figure 3. It is unrealistic to expect ten borings across the footprint of a 10 m tall embankment, but this case is included as an extreme case for model conditioning. The variability in normalized deformations for the conditional models, with or without inclusion of the site-wide statistics, is similar for the cases with 1, 2, or 3 borings (Figure 8), but does become smaller for the cases with 5 or 10 borings (Figure 9). For the conditional models based on local borings alone, the use of a single boring produced mean $(N_1)_{60cs}$ values that differed from the true mean of 15 by as much as 3 blows, but this did not significantly increase the variability in deformations because the error in the estimate mean was smaller for most of the other realizations. For conditional models based on more borings, the error in the mean $(N_1)_{60cs}$ for various realizations decreased with increasing number of borings and was generally less than one blow. The conditional models with 10 borings were relatively accurate in predicting the crest settlements of their parent models (Figure 9a), but appeared to be biased toward under-predicting their embankment stretches (Figure 9b). Conditioning on 10 borings appears to have provided an accurate representation of average foundation properties which are important for estimating crest settlements (which has a relatively large deformation mechanism), but to have smeared out local features near the embankment toes which are important for estimating embankment stretches (with the toe deformations governed by relatively small deformation mechanisms).

A comparison of the standard deviations in normalized deformations for the unconditional and conditional models indicates that the conditional models tend to produce lower standard deviations than their unconditional counterparts for analysis cases with 5 and 10 borings. The shear strains obtained at the end of shaking for PM5 with conditional models conditioned to 1, 3 and 10 borings with site-wide statistics is shown in Figure 10. An examination of the shear strains from conditional models conditioned to different numbers of borings indicate that both the deformations and the shear strain patterns approach those of the parent model with an increased number of borings. A large number of borings is required to adequately condition these models (with $\theta_x /B = 0.35$) so that the strain patterns will be similar enough to produce similar displacements as the parent model.

Embankment deformations for analysis groups 10 through 12, correspond to a foundation layer with $\theta_x = 60$ m (giving $\theta_x /B = 1.05$) and characterized by 1, 3, or 5 borings, respectively, are compared in Figure 11. These analyses are for a 10 m tall embankment, and the TCU motion scaled to a PGA of 0.6 g. The variability in the normalized deformations for the conditional models, with or without inclusion of site-wide statistics, decreases slightly as the number of borings increases from 1 to 5, and is slightly smaller than for the unconditional models when using 5 borings. Conditioning on 5 borings was more beneficial when $\theta_x = 60$ m (Figure 10) than when $\theta_x = 20$ m (Figure 9), which is attributed to deformation mechanisms for this embankment (H = 10 m, B =

57 m) being more sensitive to individual looser lenses when $\theta_x$ = 60 m, such that additional borings to identify such features produced improved estimates of deformations. For the case with $\theta_x$ = 20 m (giving $\theta_x$ /B = 0.35; Figure 9), deformations were less sensitive to individual looser lenses because there were more such lenses per embankment base width, such that the same 5 borings were not as effective in defining the extent and location of such lenses or in improving deformation estimates.

Embankment deformations for analysis groups 3 and 4 correspond to 25 m tall embankment with a foundation layer $\theta_x$ = 60 m (giving $\theta_x$ /B = 0.43) and characterized by 3 or 5 borings respectively. These analyses, which also used the TCU motion scaled to a PGA of 0.6 g, produced results similar levels of deformation variability to those for the 10 m tall embankment with $\theta_x$ = 20 m and having $\theta_x$ /B = 0.35.

***Impacts of the uncertain horizontal scales of fluctuation***

Embankment deformations for a set of conditional models based on local borings, but with imperfect estimates of $\theta_x$, were performed for conditions that otherwise are based on those for analysis group 5. These analyses were for a 10 m tall embankment with 3 local borings and the TCU motion scaled to a PGA of 0.6 g. The parent models were developed for $\theta_x$= 20 m, whereas the conditional models based on local borings were generated using $\theta_x$ of 10 m, 20 m, and 60 m. The deformations and standard deviations of deformations obtained with these models are consistent with those obtained with conditional models generated with borings from parent models with $\theta_x$ of 10 m, 20 m, and 60 m (in Figure 7). This indicates that a similar trend as was shown previously with perfect knowledge of $\theta_x$ can be produced with uncertainty in $\theta_x$.

***Impacts of ground motions***

Embankment deformations for analysis group 5 using the TCU, TAPS, and Mudurnu motions scaled to a PGA of 0.6 g are compared in Figure 12. These analyses are for a 10 m tall embankment, a foundation $\theta_x$ = 20 m, and 3 local borings. The normalized deformations with the TCU motion are more than double those for the Murdurnu motion, which reflects their differences in duration and frequency content. The relative differences in normalized deformations obtained with conditional versus unconditional models show no discernable trends with ground motion. These results suggest that the previous observations regarding the use of conditional versus unconditional models are not sensitive to individual ground motions.

**Accuracy and uncertainty of deformation predictions from conditional models**

The average efficiency index is plotted in Figure 13 versus the average absolute error in normalized deformations relative to the parent model for each set of conditional models with the 10 m, 25 m, and 45 m embankments. The average efficiency index (Li et al. 2016) is,

$$I_{avg} = \frac{\sigma_{\ln(u)}}{\sigma_{\ln(c)}} \quad \text{(eqn. 1)}$$

where $\sigma_u$ = standard deviation of the unconditional models and $\sigma_c$ = standard deviation of the conditional models. The average absolute error in normalized deformations is the average of the absolute errors for each conditional model relative to the parent model,

$$D_i = \frac{|d_{CMi} - d_{PM}|}{d_{PM}} * 100 \quad \text{(eqn. 2)}$$

where $D_i$ = absolute error for conditional model i relative to its parent model, $d_{CMi}$ = normalized deformation of conditional model i, and $d_{PM}$ = normalized deformation of the associated parent model. The different symbols in this figure distinguish between analysis sets based on the level of knowledge (symbol size), normalized scales of fluctuation (symbol shape), and number of borings (symbol color).

The trends in Figure 13 indicate that as the number of borings increases, the average absolute error decreases and the average efficiency index increases, meaning that the deformation distribution converges toward the deformations of the parent model with increased conditioning. For crest settlements (Fig. 13a), the results for 5 and 10 borings (blue and purple symbols) generally show errors (5-30%) and efficiencies ($I_{avg}$ of 1-3) that are better than for 1, 2, or 3 borings (red, yellow, and green symbols, respectively) where errors are as high as 70% and efficiencies range from about 0.7 to 2.5. For embankment stretches (Fig. 13b), the results for 5 and 10 borings also show reductions in the absolute errors relative to 1, 2, or 3 borings, but the improvement is not as significant and the efficiencies are more variable. There is also a slight trend of increasing $I_{avg}$ with increased $\theta_x$ which reflects the larger $\sigma_{\ln(u)}$ that occurs with larger $\theta_x$. The $I_{avg}$ values are approximately0.2-0.3 for crest settlement and stretch for the 45 m embankment (i.e., $\theta_x/B$ =0.08) and 0.3-0.6 for crest settlement for the 25 m embankment with $\theta_x$ = 20 m (i.e., $\theta_x/B$ =0.14). These latter cases correspond to the smallest $\theta_x/B$ considered in these analyses and suggest the conditional models can be more variable than the unconditional models when $\theta_x/B$ is less than about 0.14. However, these latter cases have the smallest $\sigma_{ln(u)}$ such that their correspondingly larger $\sigma_{ln(c)}$ is still small relative to those obtained for larger $\theta_x/B$ values (e.g., for the 10 m embankments or for the 25 m embankments with $\theta_x$ = 60 m) as shown in Fig. 6.

The average efficiency index is plotted in Figure 14 versus the average error in normalized deformations relative to the parent model for each of set of conditional models with the 10 m embankment. The different symbols in this figure, as for Figure 13, distinguish between analysis sets based on the level of knowledge, normalized scales of fluctuation, and number of borings. The average error in this figure would be zero for a set of conditional model predictions that are unbiased relative to the parent model. Thus, the distribution of points with positive and negative average errors illustrate that the conditional models both over and under predicted the deformations of parent models. The general trend in this figure, similar to that for Figure 13, indicates that as the number of borings increases, the average error generally reduces towards zero and the average efficiency index increases. However, the gains are modest even for conditioning on 5 or 10 borings. There is also a slight trend of increasing $I_{avg}$ with increased $\theta_x$ which reflects the larger $\sigma_{ln(u)}$ that occurs with larger $\theta_x$.

The average difference (or error) in normalized deformations relative to the mean of the corresponding unconditional models for sets of conditional analyses are plotted in Fig. 15 versus the average error in normalized deformations relative to the parent model. The different symbols in this figure, like for Figs. 13 and 14, distinguish between analysis sets based on level of knowledge, normalized scales of fluctuation and number of borings. For crest settlements (Fig. 15a), the results for conditional models with 1, 2, or 3 borings (red, yellow, and green symbols) tend to have average differences relative to the mean from the corresponding unconditional models that are smaller than the average errors relative to the parent models; e.g., the majority of points plot between -30% and +20% relative to the mean of the unconditional models and between -50% and +70% relative to the parent models. The crest settlement results for conditional models with 5 or 10 borings (blue and purple symbols) have smaller errors/differences relative to the parent model (-25% to +15%) than relative to the mean of the corresponding unconditional models (-30% to +30%). This trend indicates that the crest deformations tend to converge toward the parent model deformations as the number of borings is increased, even if the parent model deformations are significantly greater than or smaller than the mean for the unconditional models. A similar trend is evident in the results for embankment stretches (Fig. 15b). Overall, these results suggest that conditioning on a small number of borings produces results that are similar to those for unconditional models (given they were generated with similar geostatistical parameters), and that a large number of borings (e.g., 5 or 10) is needed to significantly reduce potential errors relative to the parent model (i.e., the true case).

**Discussion**

The observation that the benefits of conditional models for predicting embankment deformations depend on the scale of fluctuation relative to the scale of the embankment (e.g., $\theta_x/B$) and the number of samples used to condition the model is consistent with expectations based on prior studies for other types of geotechnical sampling (e.g., Baecher and Ingra 1981, Fenton and Griffiths 2008, Joint TC205/TC304 Working Group 2017). It is likely that the efficacy of conditional models will be affected to various degrees by factors not examined herein (e.g., sample spacing in the vertical direction; sample locations; hydraulic conductivities; reservoir level; stochastic modeling framework; constitutive models; three-dimensional effects), in addition to those factors examined in the sensitivity studies (e.g., ground motion characteristics, system geometries). Precisely quantifying these secondary dependencies and their cross-correlations would take many times more simulations than were possible in the current study given the computational and manual interpretation demands. Nonetheless, the trends in the results presented herein are sufficient to demonstrate that the potential benefits of conditional models for assessing liquefaction effects depend on the expected deformation mechanisms, scales of an embankment, scales of fluctuation, and number of samples in the liquefiable strata.

The use of site-wide statistics as an aid in the conditioning of models did not significantly improve the accuracy of embankment deformation predictions in the present study, but this observation should not be generalized. The present analyses mostly assumed that the conditional models based on local borings also had perfect knowledge of $\theta_x$, which would only come from a well-informed understanding of the depositional processes based on a site-wide study. Analyses that included imperfect knowledge of $\theta_x$ produced similar trends to those obtained with perfect knowledge of $\theta_x$. Two or more local borings were generally sufficient for obtaining reasonably accurate estimates of the mean $(N_1)_{60cs}$, COV, and $\theta_y$ for the foundation layer because the stratum was relatively thick and it was modeled with stationary properties. In cases where the statistics of the stratum are not stationary, subdividing the stratum based on the local statistics may provide a better assessment of potential deformations.

Conditional models were generally more effective at improving deformation predictions when the horizontal scale of fluctuation was approximately equal to the base width of the embankment ($\theta_x/B \approx 1$). In this case, a set of three or more borings were generally more effective at identifying looser zones that were long enough to influence embankment crest settlements. If a lengthy zone of significantly looser soils is evident in the borings at a cross-section, they will be reflected in the conditional realizations or, alternatively, may be deterministically considered as separate substrata in practice.

Characterizing spatial variability in alluvial strata or other types of deposits requires a detailed geologic model and understanding of site-specific depositional processes. The geologic model provides a basis for identifying different strata that may have significantly different stochastic properties (e.g., property distributions or scales of fluctuation), and thus avoids the potentially obscuring effect of representing two or more distinctly different strata with one set of geostatistical parameters. The geologic model also provides a basis for refining site investigation studies, assessing stationarity of soil properties, evaluating the potential for certain types of geologic features to have been missed by the site explorations, and constraining estimates of property distribution and scales of fluctuation beyond what may be estimated using site exploration data alone. In order for conditional NDAs to be valuable in estimating deformations, their value is contingent on the geologic model and site investigation data being reasonably accurate.

## Conclusions

Two-dimensional NDAs of hypothetical embankment dams on spatially variable liquefiable foundation layers were used to evaluate the utility of representing the foundation layer with random fields conditioned on different levels of site characterization information. Parent models representing a "true" foundation condition were generated using unconditional random fields of $(N_1)_{60cs}$ values for given sets of site-wide geostatistical properties. Different levels of site characterization were represented by combining different numbers of local borings (i.e., columns of data from the parent model) with optional constraints on the geostatistical properties that might come from the site-wide explorations and geologic studies. NDAs were performed for the parent model (which represents perfect knowledge of soil conditions at a given cross-section) and sets of realizations conditioned on the local borings with or without knowledge of the site-wide statistics. Embankment deformations obtained for the conditioned realizations are compared to those for the parent model to evaluate the relative impacts of increasing levels of site characterization on the accuracy of deformation predictions. The key assumption is that factors that impact results from an NDA model with an unconditional random field representing the $(N_1)_{60cs}$ values in the foundation alluvium will have approximately equal impacts on results from an NDA model with all other aspects the same except for the conditioning of the random field. At the same time, it is unlikely that any quantitative evaluation of potential reductions in bias or dispersion through the use of conditional realizations can be generalized for application in practice, as the dispersion in deformations is itself significantly affected the nature and distributions of properties in the embankment and foundation and the nature of the loading. The number of realizations and ground motions presented in the following sections are therefore considered sufficient, for comparative purposes, to qualitatively identify whether there was a marked reduction in the variability of calculated deformations.

The potential benefits of conditioning stochastic realizations on borings at a specific cross-section of a water-retention embankment were not very strong, although these observations should not be generalized outside the limited range of conditions examined herein. The conditioning of stochastic realizations using only 1, 2 or 3 borings for the 12-m thick foundation layer, with or without inclusion of site-wide geostatistical information, produced crest settlements and overall embankment stretches (sum of outward toe displacements) in 10 m, 25 m, and 45 m tall embankments that were similar to those obtained for unconditional stochastic realizations models generated with similar geostatistical parameters. Conditioning using only 1, 2, or 3 borings did not substantially improve predictions of the true parent model's deformations, particularly for more localized deformations near the embankment toes. Improvements in accuracy and efficiency for predicting the true parent model's deformations were obtained when the stochastic realizations for the foundation of a 10 m tall embankment were conditioned on 5 or 10 borings, with the greatest improvements in efficiency generally coming from cases with $\theta_x/B \approx 1$. However, the benefits were modest given that this number of borings near a single cross-section is unlikely for this size embankment. These observations are generally consistent with findings regarding the use of conditional models for other geotechnical applications, as summarized in Joint TC205/TC304 Working Group (2017) and Liu et al. (2017), and provide insights on the benefits and limitations of conditional stochastic modeling for NDAs of levees or embankment dams on liquefiable soils.

A primary benefit of additional exploration work is supporting development of an accurate geologic model and reducing the potential for missing key features that could lead to significant bias in NDA results. In the present study, the incremental benefits of additional borings (within practical limitations) were generally small when comparing deformation results from unconditioned and conditioned models, but these results are for situations where the primary features of the alluvial layer were reasonably well constrained. In practice, detailed explorations and an accurate geologic model are essential for assessing liquefaction effects on embankments and other infrastructure, as they provides a basis to identify distinctly different strata, assess the possibility that important geologic features have been missed, assess the potential stationarity of soil properties, and constrain estimates of soil property distributions, whether stochastic modeling tools are used or not.

**Data Availability Statement**

Data that support the findings of this study are available from the corresponding author upon reasonable request.

**Acknowledgements**

The work described herein progressed under projects for the California Department of Water Resources under Contract 4600009751 and the National Science Foundation under grant CMMI-1635398. Any opinions, findings, conclusions, or recommendations expressed herein are those of the authors and do not necessarily represent the views of these organizations. Professor Jack Montgomery provided assistance with the initial stochastic modeling. The anonymous reviewers provided suggestions that improved the paper. The authors appreciate the above for their support and assistance.

## References

Ancheta, T. D., Darragh, R. B., Stewart, J. P., Seyhan, E., Silva, W. J., Chiou, B. S. J., et al. (2014). NGA-West2 database. Earthquake Spectra EERI 2014; 30(3):989-1005.

Baecher, G. B., and Ingra, T. S., (1981). "Stochastic FEM in settlement predictions." Journal of Geotechnical Engineering, ASCE, 107(4), 449-464.

Boulanger, R. W., and Beaty M. H., (2016). "Seismic Deformation Analyses of Embankment Dams: A Reviewer's Checklist", In Proc., 36th USSD Annual Meeting and Conference, United States Society on Dams, 2016. 535-546.

Boulanger, R. W., and Idriss, I. M. (2012). "Probabilistic SPT-based liquefaction triggering procedure." Journal of Geotechnical and Geoenvironmental Engineering, ASCE, 138(10), 1185-1195.

Boulanger, R. W., and Montgomery, J. (2016). "Nonlinear deformation analyses of an embankment dam on a spatially variable liquefiable deposit." Soil Dynamics and Earthquake Engineering, 91, 222–233.

Boulanger, R. W., and Ziotopoulou, K. (2017). "PM4Sand (Version 3.1): A sand plasticity model for earthquake engineering applications", rep. No. UCD/CGM-17/01, Center for Geotechnical Modeling, Dept. of Civil and Environmental Engineering, Univ. of California, Davis, CA.

Constantine, P. G., and Wang, Q. (2012). "Random field simulation." http://www.mathworks.com/matlabcentral/fileexchange/27613-random-field-simulation, Accessed January 2017.

Davis, M. (1987). "Production of conditional simulations via the LU triangular decomposition of the covariance matrix." Mathematical Geology, 19(2):91-98.

Duncan, J. M., and Wright, S. G. (2005). Soil strength and slope stability. J. Wiley & Sons, Hoboken.

Fenton, G. A., and Griffiths, D. V. (2008). Risk Assessment in Geotechnical Engineering. John Wiley & Sons, Inc., New York.

Fenton, G. A., Griffiths, D. V., Williams, M. B. (2005). "Reliability of traditional retaining wall design." Géotechnique, 55(1), 55-62.

Griffiths, D. V., Fenton, G. A., Manoharan, N. (2006). "Undrained bearing capacity of two-strip footings on spatially random soil." ASCE International Journal of Geomechanics,6(6), 421-427.

Itasca (2016). Fast Lagrangian Analysis of Continua (FLAC), release 8.0. Itasca Consulting Group, Inc., Minneapolis, MN.

Johnson, R. A., and Bhattacharyya, G. K. (2010). Statistics Principles and Methods. J. Wiley & Sons, Hoboken.

Joint TC205/TC304 Working Group (2017). "Discussion of statistical/reliability methods for Eurocodes – Final Report." 5th International Symposium on Geotechnical Safety and Risk, International Society for Soil Mechanics and Geotechnical Engineering, Rotterdam, Netherlands, 2015.

Li, Y. J., Hicks, M. A. and Vardon, P. J. (2016). "Uncertainty reduction and sampling efficiency in slope designs using 3D conditional random fields." Computers and Geotechnics, 79:159-172.

Liu, L., Cheng, Y., and Zhang, S., (2017). "Conditional random field reliability analysis of a cohesion-frictional slope." Computers and Geotechnics, 82:173-186.

Mejia, K. H., and Dawson, E. M. (2006). "Earthquake Deconvolution for FLAC." 4th International Symposium on Numerical Modeling in Geomechanics, Minneapolis, MN.

Montgomery, J., Boulanger, R. W., Armstrong, R. J., and Malvick, E. J. (2014). "Anisotropic Undrained Shear Strength Parameters for Nonlinear Deformation Analyses of Embankment Dams." Geo-Congress 2014 Technical Papers.

Paull, N. A., Boulanger, R. W., and DeJong, J. T. (2019). "Seismic deformations of different size embankments on a spatially variable liquefiable deposit." Proc., 39th USSD Annual Meeting and Conference, United States Society on Dams, Chicago, IL, 2019.

Paull, N. A., Boulanger, R. W., and DeJong, J. T. (2020). "Nonlinear Deformation Analyses of Embankments on a Spatially Variable Liquefiable Deposit Using

Conditional Random Fields.” Geo-Congress 2020 Technical Papers, Minneapolis, MN, 2020.

Phoon, K.-K., and Kulhawy, F. H. (1999). “Characterization of geotechnical variability.” Canadian Geotechnical Journal, 36(4), 612–624.

URS (2012). “Seismic Deformation Analysis with UBCSAND”. California Department of Water Resources. Sacramento, CA.

Vanmarcke, E. (2010). Random fields: analysis and synthesis. World Scientific, Hackensack, NJ.

Ziotopoulou, K., and Boulanger, R. W. (2016). "Plasticity modeling of liquefaction effects under sloping ground and irregular cyclic loading conditions." Soil Dynamics and Earthquake Engineering, 84 (2016), 269-283, 10.1016/j.soildyn.2016.02.013.

Table 1: Properties for embankment analysis groups. Each analysis group uses three parent models and two knowledge classifications.

| Analysis group | Embankment height, H (m) | Embankment base length, B (m) | Horizontal scale of fluctuation, $\theta_x$ (m) | Normalized scale of fluctuation, $\theta_x/B$ | Number of borings, $N_b$ |
|---|---|---|---|---|---|
| 1 | 45 | 249 | 20 | 0.08 | 3 |
| 2 | 25 | 138 | 20 | 0.14 | 3 |
| 3 | 25 | 138 | 60 | 0.43 | 3 |
| 4 | 25 | 138 | 60 | 0.43 | 5 |
| 5 | 10 | 57 | 20 | 0.35 | 3 |
| 6 | 10 | 57 | 20 | 0.35 | 2 |
| 7 | 10 | 57 | 20 | 0.35 | 1 |
| 8 | 10 | 57 | 20 | 0.35 | 5 |
| 9 | 10 | 57 | 20 | 0.35 | 10 |
| 10 | 10 | 57 | 60 | 1.05 | 5 |
| 11 | 10 | 57 | 60 | 1.05 | 3 |
| 12 | 10 | 57 | 60 | 1.05 | 1 |
| 13 | 10 | 57 | 10 | 0.17 | 3 |

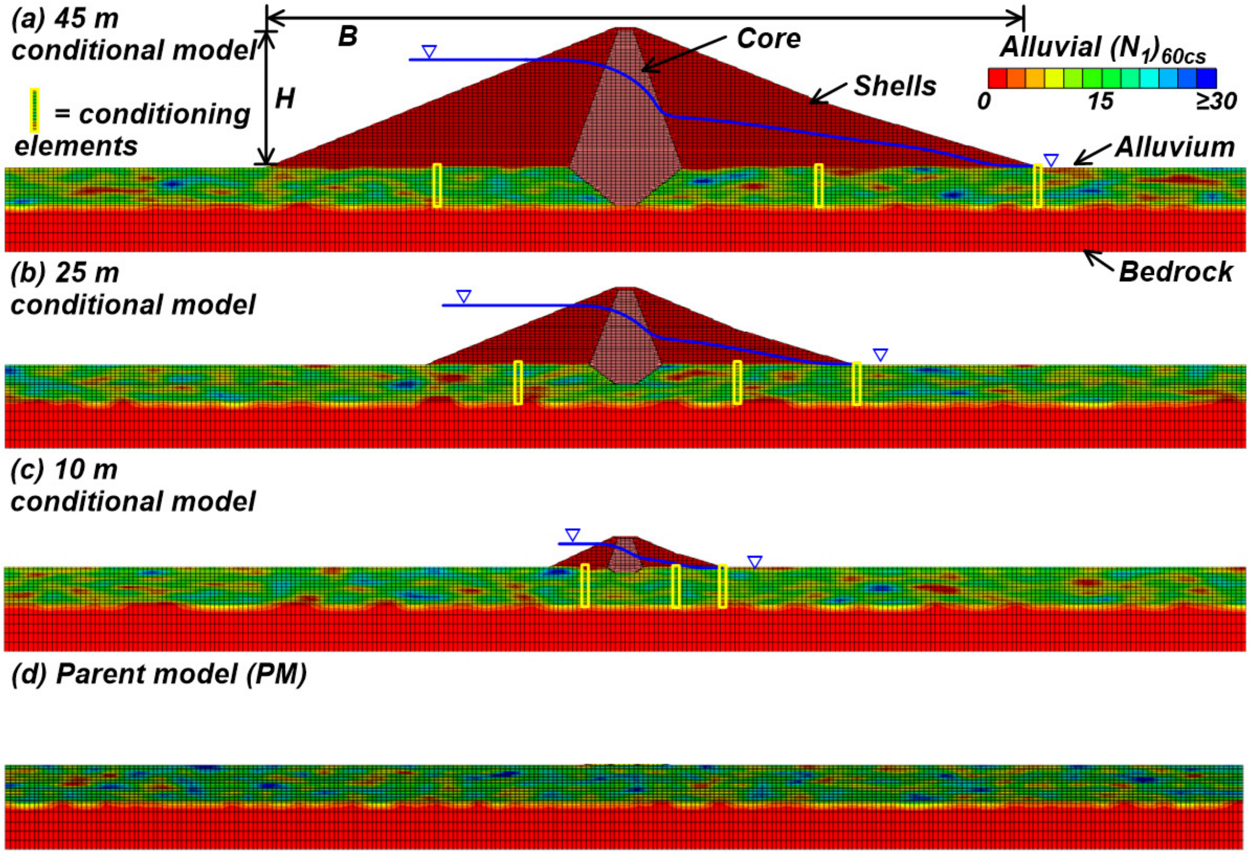


Figure 1. Embankment models with foundation layer realizations conditioned on three local borings: (a) 45 m high embankment, (b) 25 m high embankment, (c) 10 m high embankment, and (d) parent model for the liquefiable foundation layer.

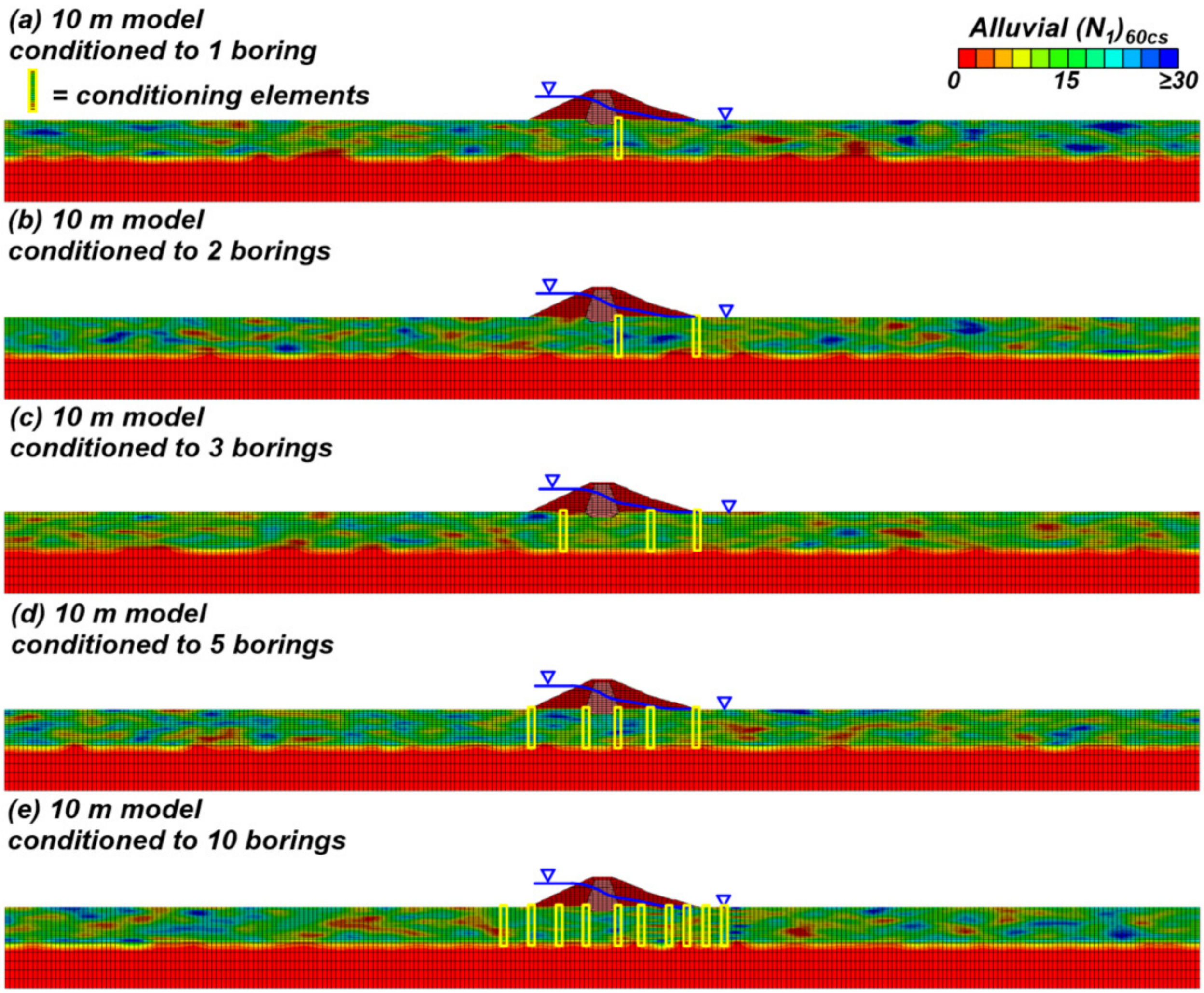

Figure 2. A 10 m tall embankment on foundation layer realizations conditioned to (a) 1 boring, (b) 2 borings, (c) 3 borings, (d) 5 borings and, (e) 10 borings.

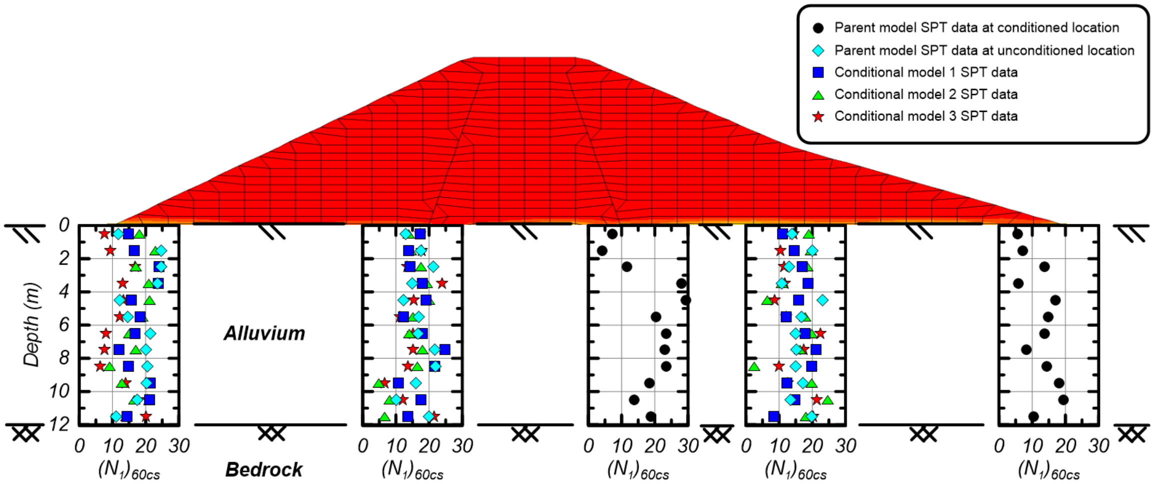


Figure 3. Profiles of SPT values for a 10 m tall embankment on three foundation layer realizations that were conditioned based on two local borings and site-wide statistics.

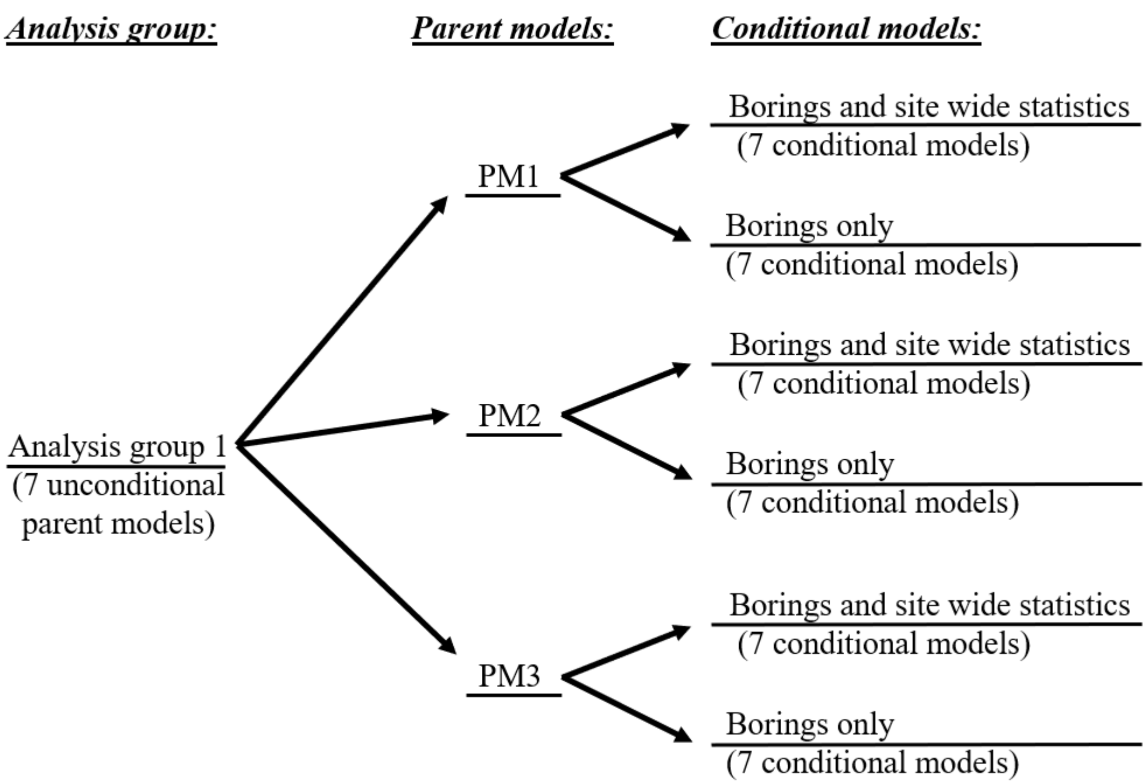


Figure 4: Analysis cases for analysis group 1.

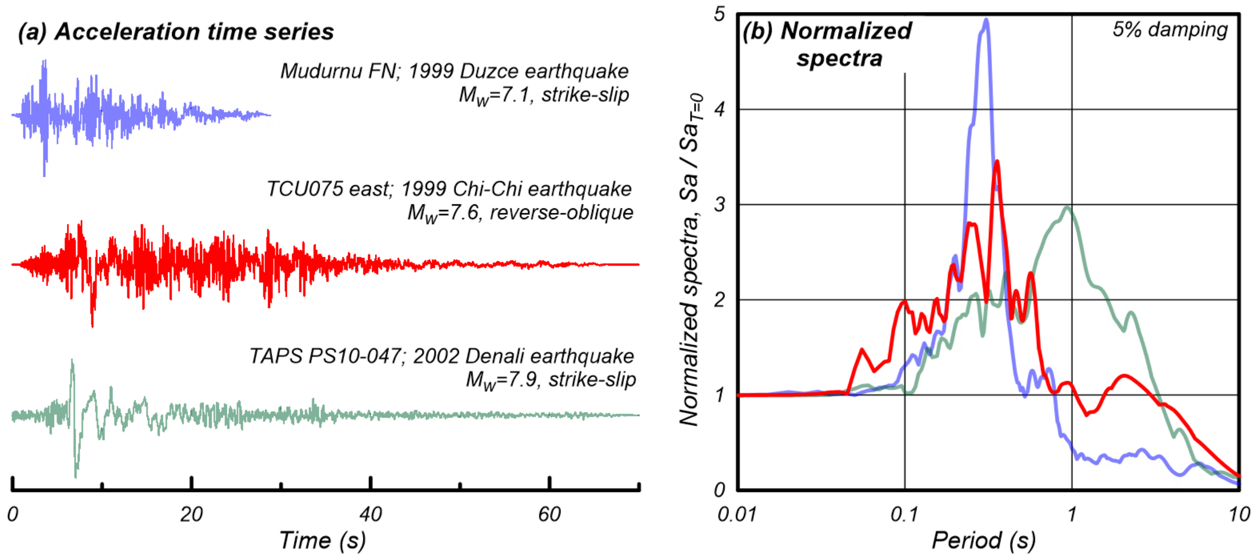


Figure 5: (a) Acceleration time series and (b) normalized spectra for input motions (After Boulanger and Montgomery 2016).

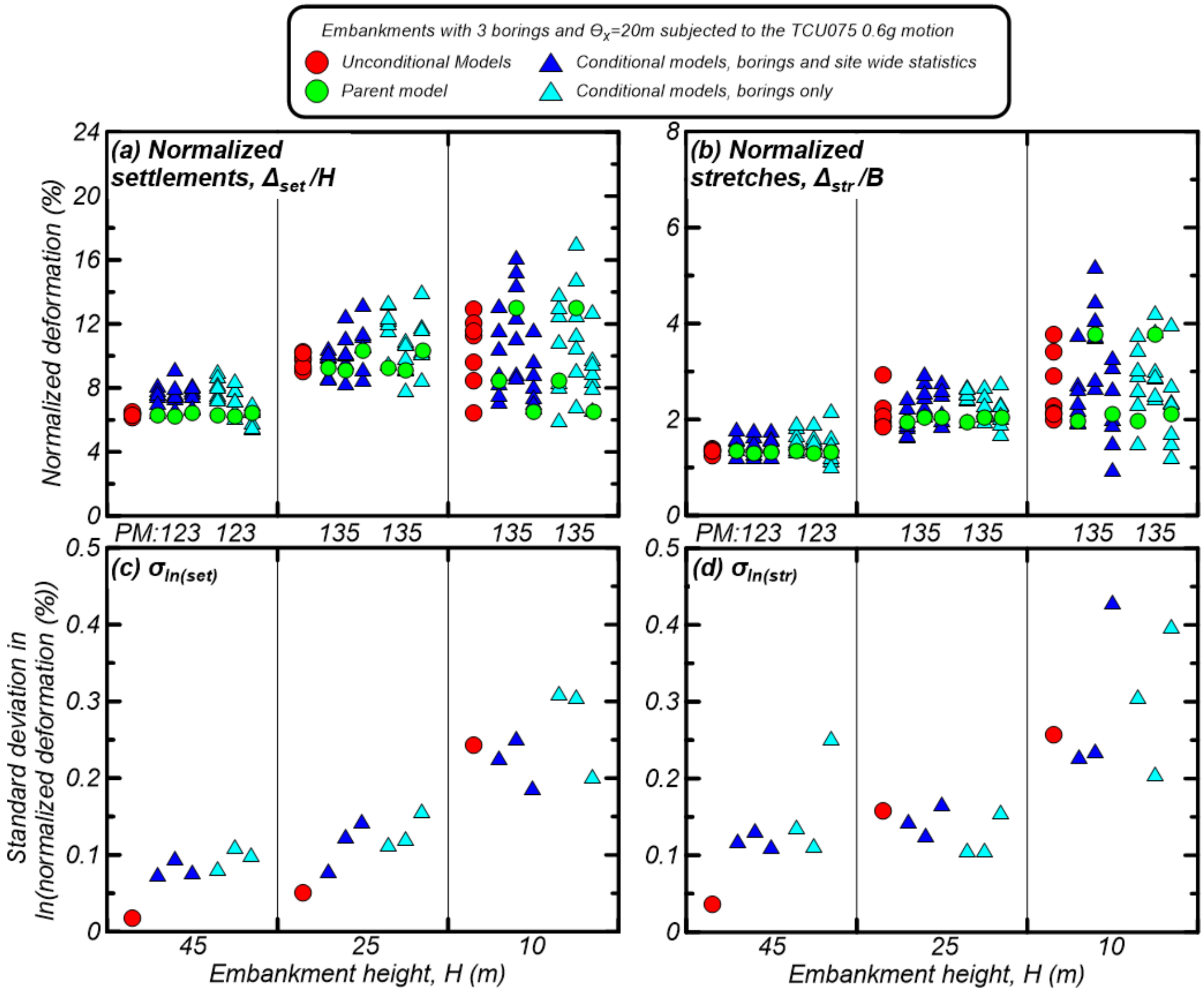


Figure 6: (a) Normalized crest settlements, (b) Normalized embankment stretches, (c) standard deviations of ln(normalized crest settlements (%)) and (d) standard deviations of ln(normalized embankment stretches (%)) for the 45 m, 25 m and 10 m embankment models subjected to the TCU motion scaled to a PGA of 0.6 g with unconditional and conditional realizations of alluvial $(N_1)_{60cs}$.

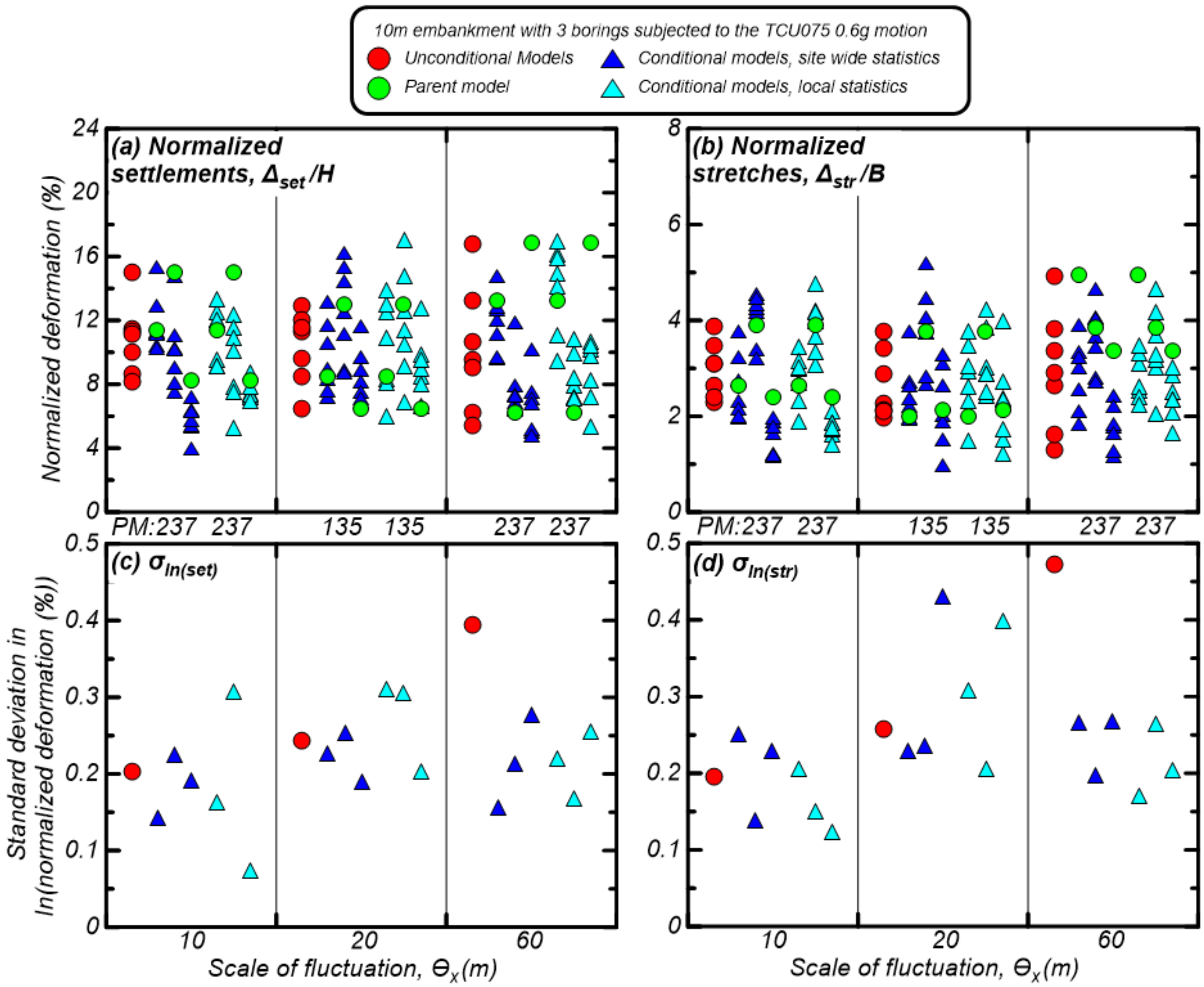


Figure 7: (a) Normalized crest settlements, (b) Normalized embankment stretches, (c) standard deviations of ln(normalized crest settlements (%)) and (d) standard deviations of ln(normalized embankment stretches (%)) for the 10 m embankment models subjected to the TCU motion scaled to a PGA of 0.6 g with unconditional and conditional realizations of alluvial $(N_1)_{60cs}$ with various horizontal scales of fluctuation.

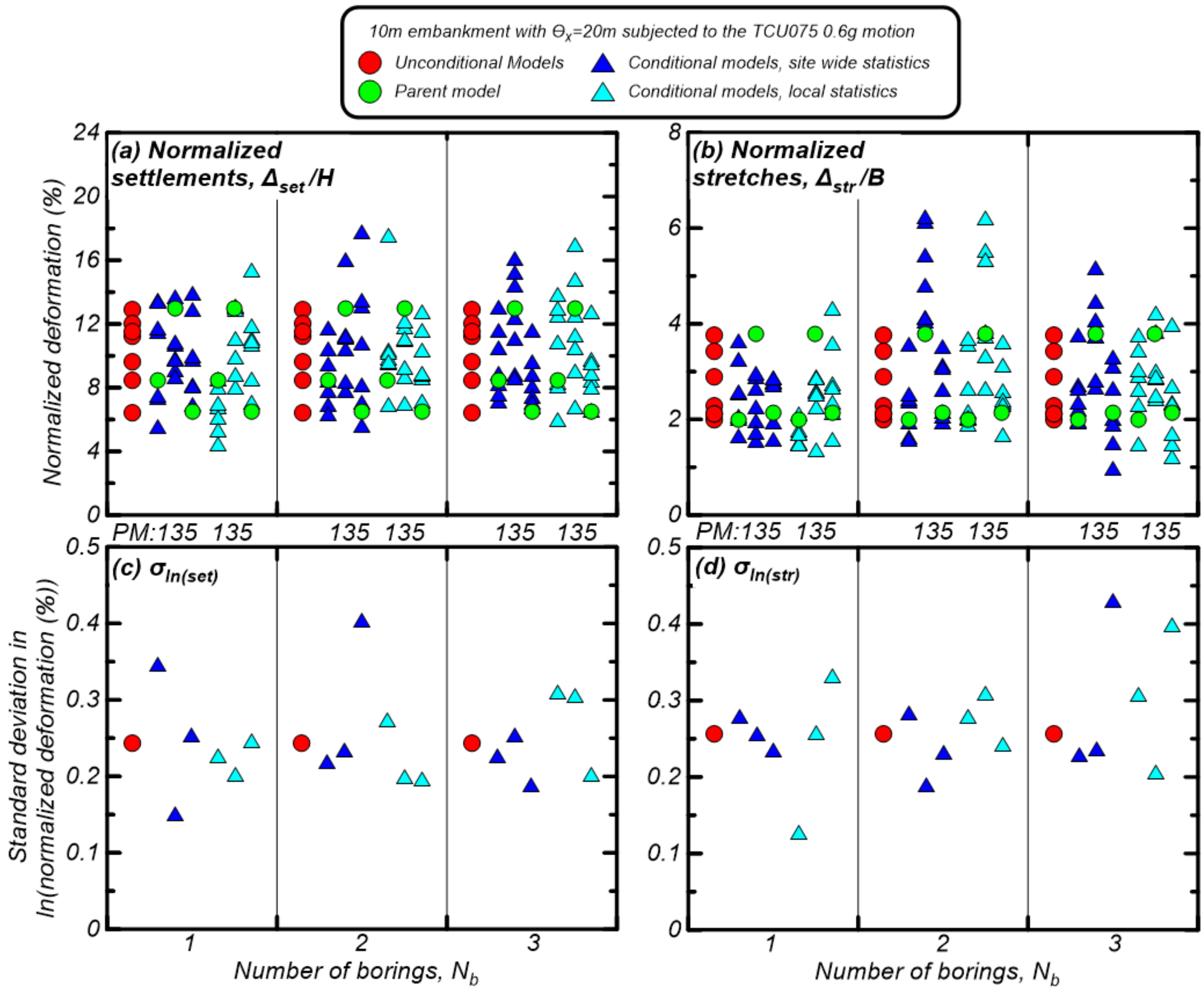


Figure 8: (a) Normalized crest settlements, (b) Normalized embankment stretches, (c) standard deviations of ln(normalized crest settlements (%)) and (d) standard deviations of ln(normalized embankment stretches (%)) for the 10 m embankment models subjected to the TCU motion scaled to a PGA of 0.6 g with unconditional and conditional realizations of alluvial $(N_1)_{60cs}$ with various numbers of conditional borings.

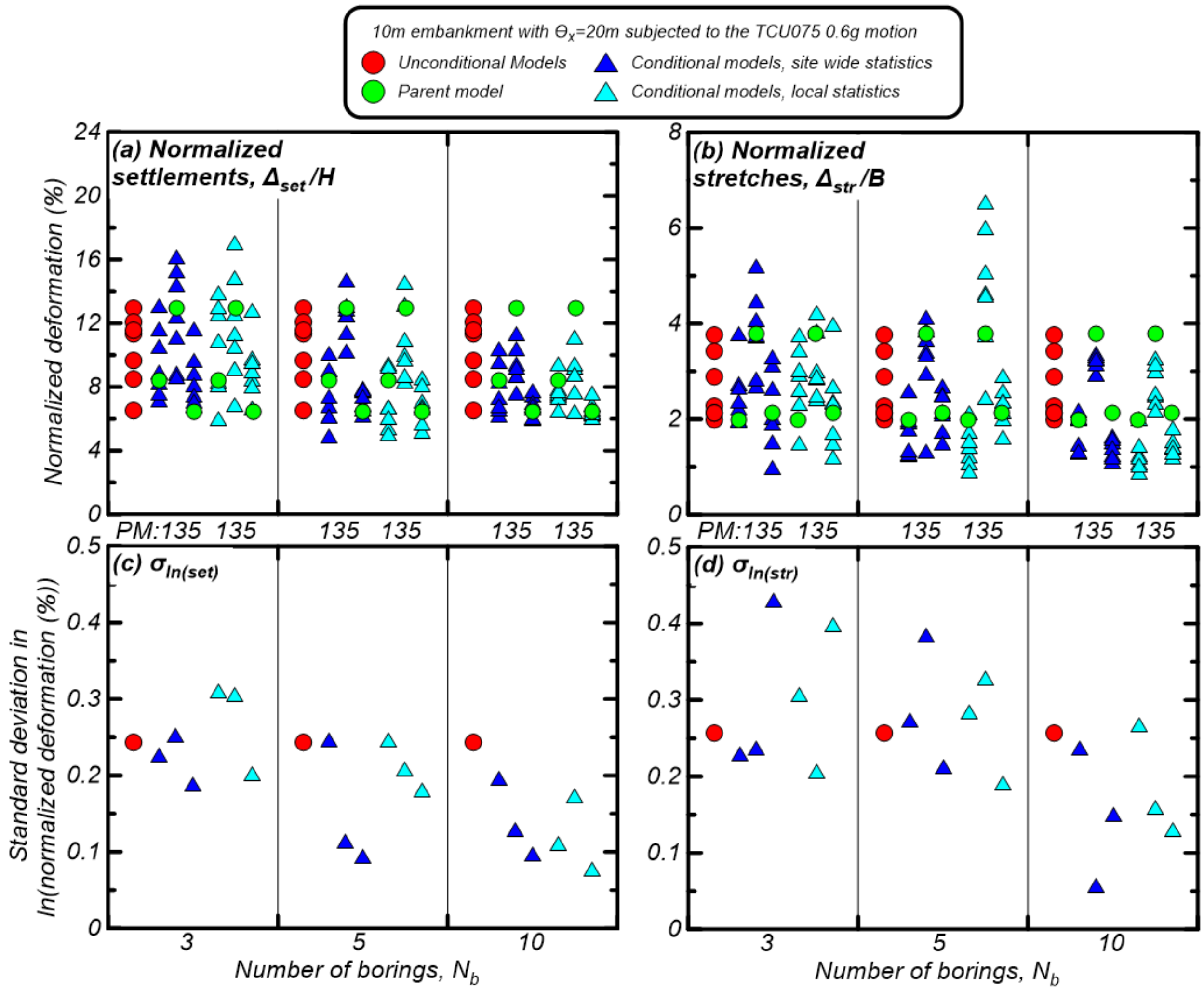


Figure 9: (a) Normalized crest settlements, (b) Normalized embankment stretches, (c) standard deviations of ln(normalized crest settlements (%)) and (d) standard deviations of ln(normalized embankment stretches (%)) for the 10 m embankment models subjected to the TCU motion scaled to a PGA of 0.6 g with unconditional and conditional realizations of alluvial $(N_1)_{60cs}$ with various numbers of conditional borings.

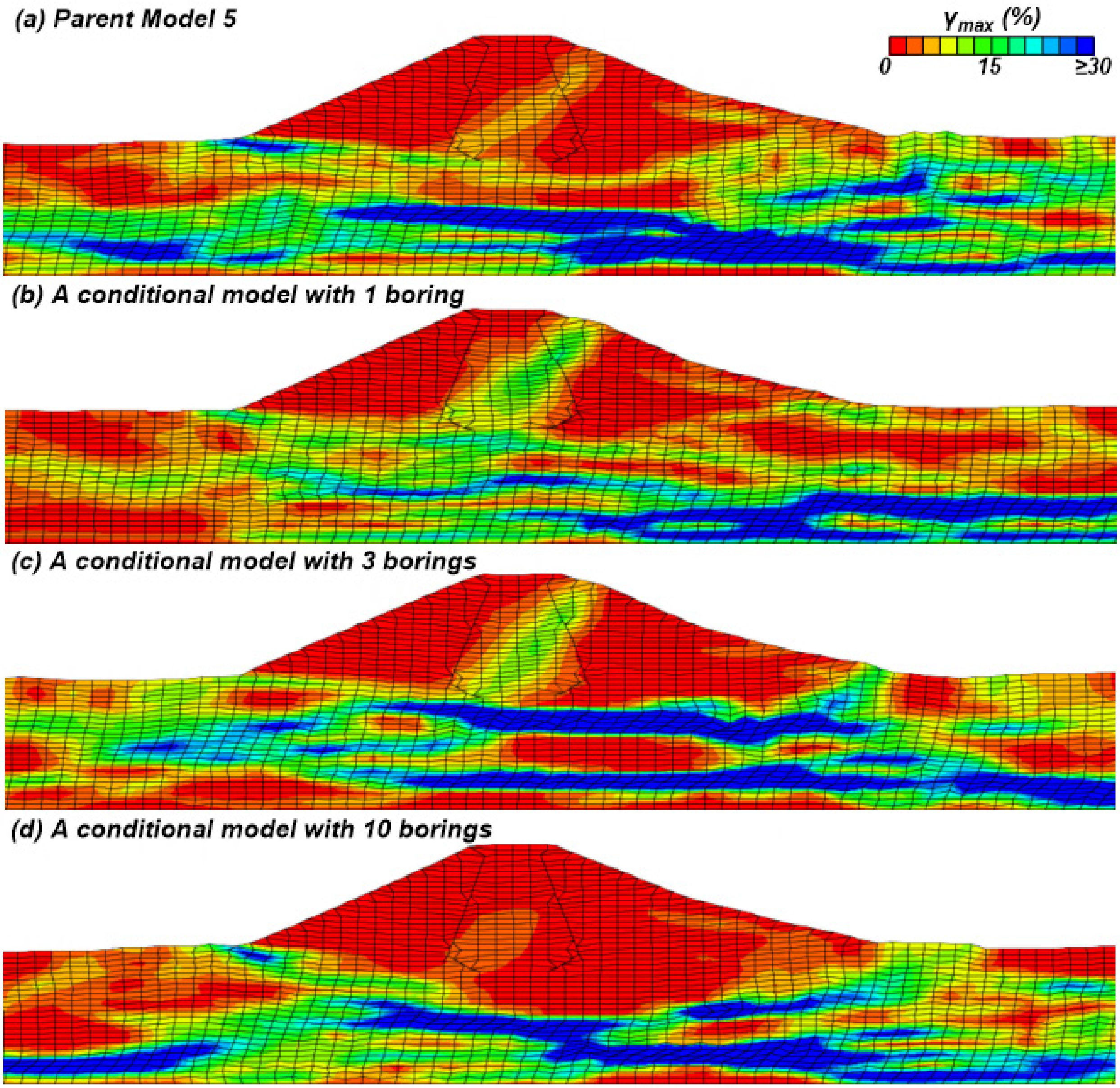


Figure 10: Shear strains from (a) Parent Model 5, (b) site wide statistics and 1 conditional boring, (b) site wide statistics and 3 conditional borings, (b) site wide statistics and 10 conditional borings for the 10 m embankment subjected to the TCU motion with a PGA of 0.6 g. The locations of conditional borings can be seen in Figure 2.

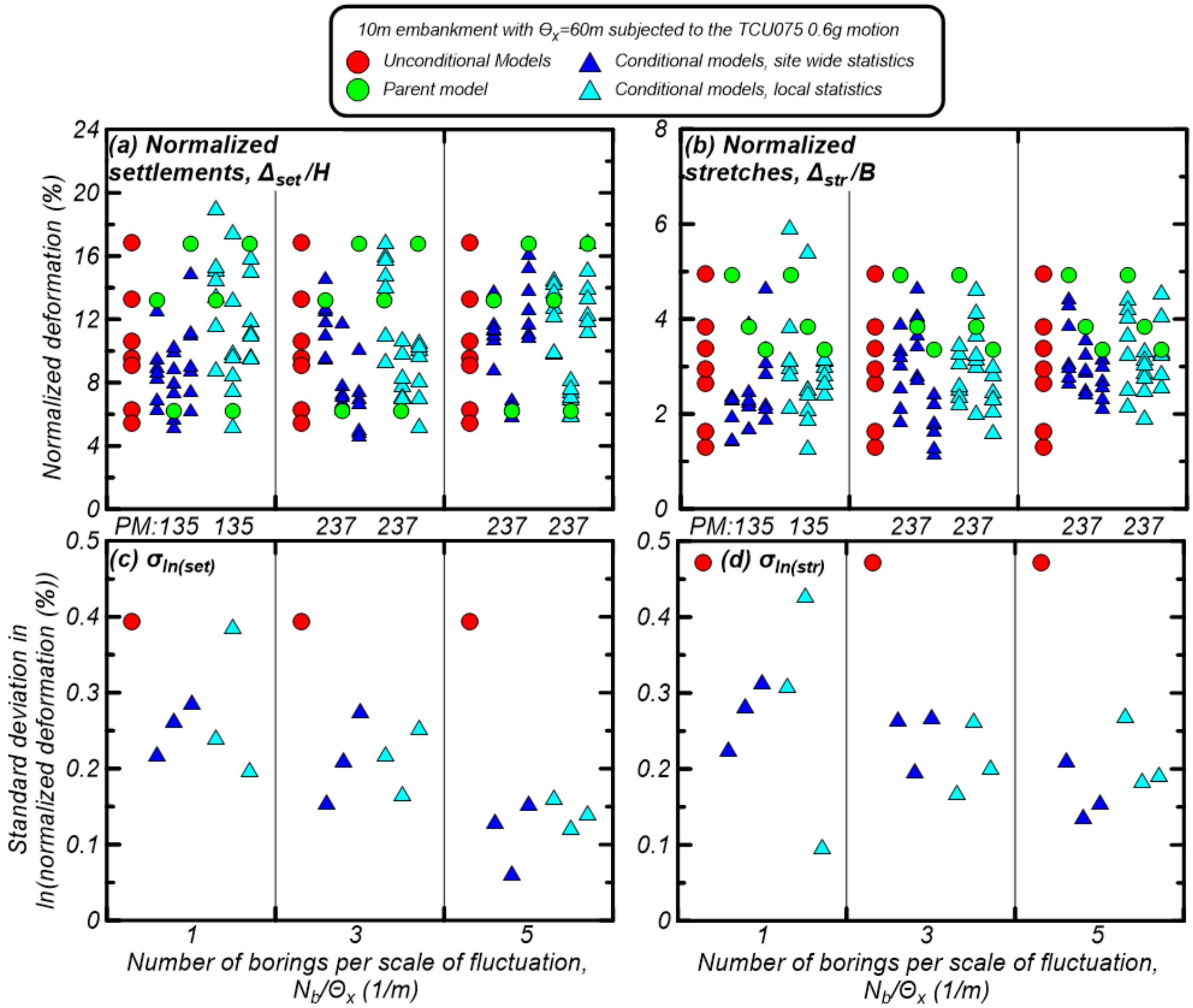


Figure 11: (a) Normalized crest settlements, (b) Normalized embankment stretches, (c) standard deviations of ln(normalized crest settlements (%)) and (d) standard deviations of ln(normalized embankment stretches (%)) for the 10 m embankment models subjected to the TCU motion scaled to a PGA of 0.6 g with unconditional and conditional realizations of alluvial $(N_1)_{60cs}$ with various numbers of borings per horizontal scale of fluctuation.

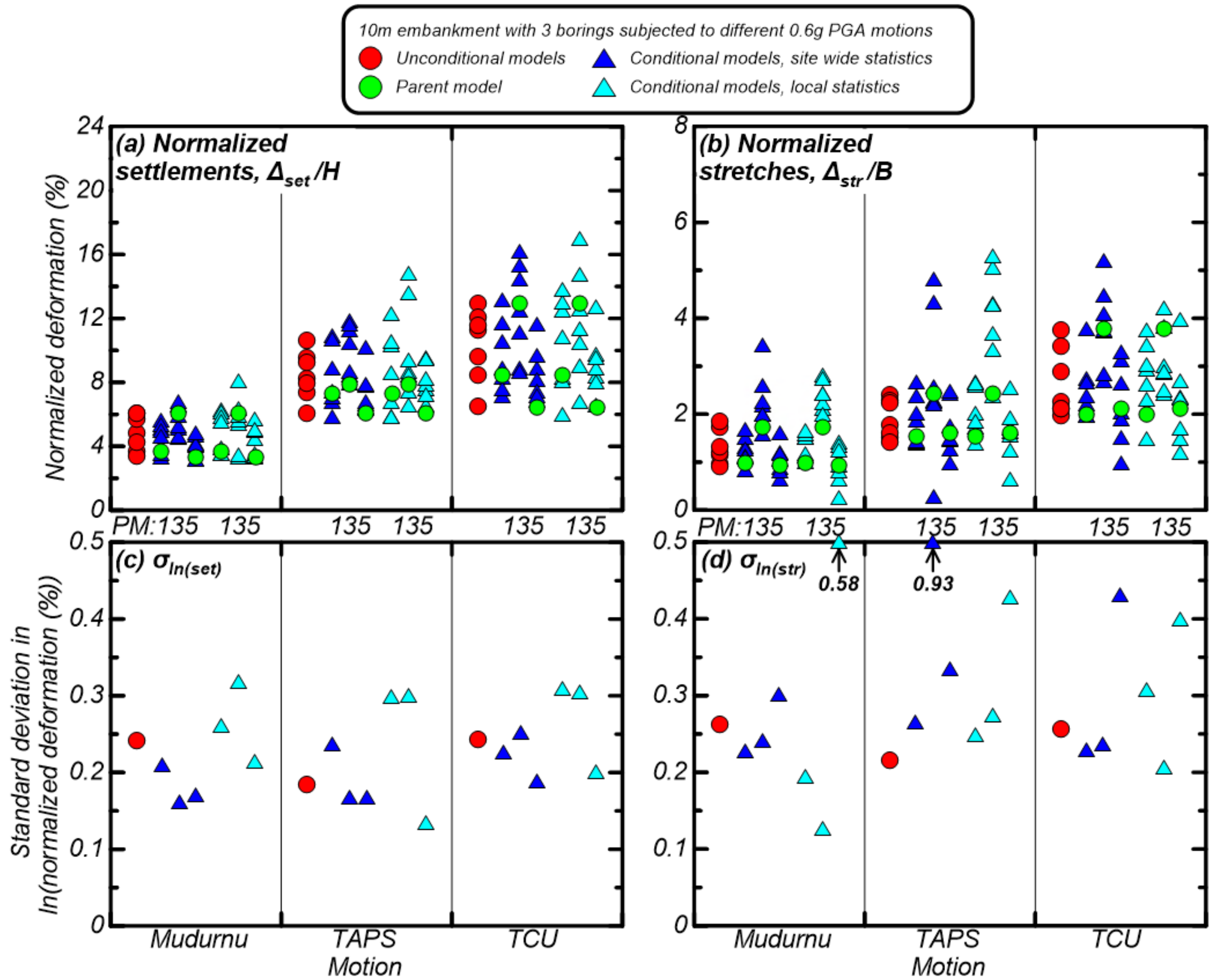


Figure 12: (a) Normalized crest settlements, (b) Normalized embankment stretches, (c) standard deviations of ln(normalized crest settlements (%)) and (d) standard deviations of ln(normalized embankment stretches (%)) for the 10 m embankment models with uniform, unconditional and conditional realizations of alluvial $(N_1)_{60cs}$ for different ground motions scaled to a PGA of 0.6 g.

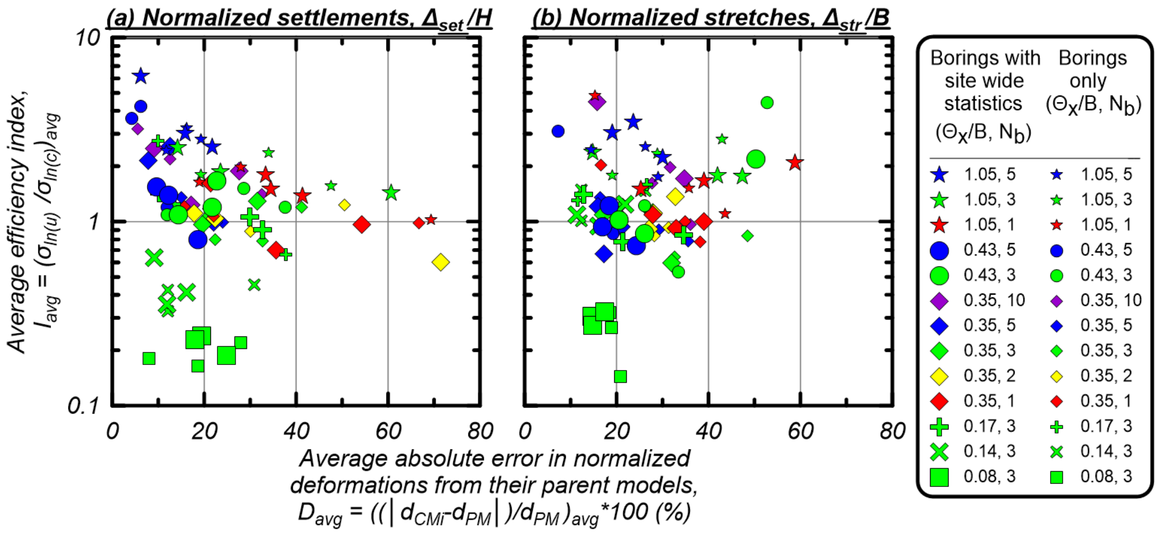


Figure 13: Average efficiency index for sets of conditional analyses plotted against the average absolute error in normalized deformations relative to the parent model for (a) normalized settlements and, (b) normalized stretches.

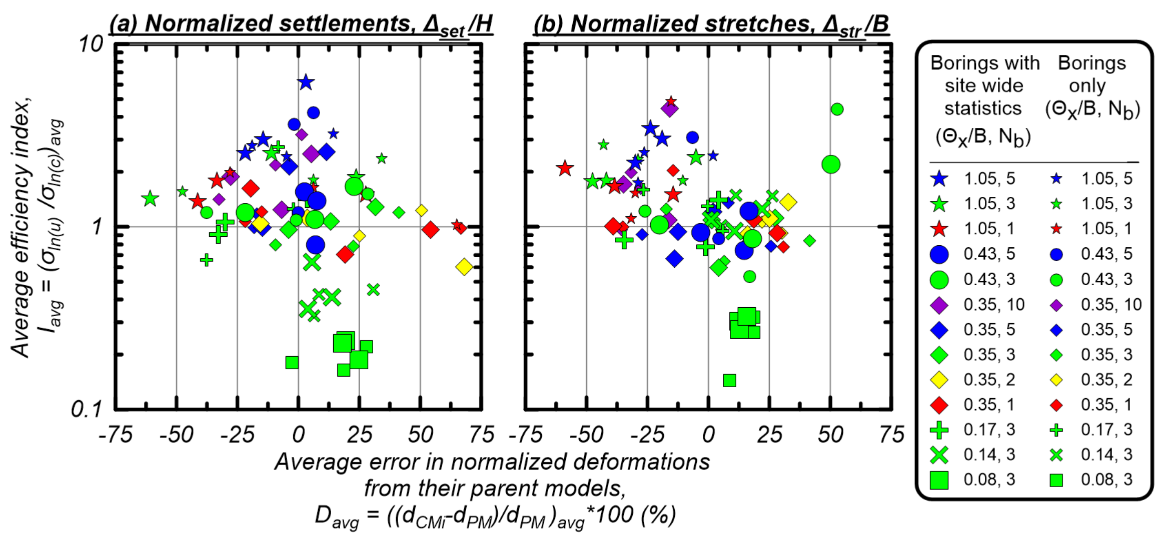


Figure 14: Average efficiency index for sets of conditional analyses plotted against the average error in normalized deformations relative to the parent model for (a) normalized settlements and, (b) normalized stretches.

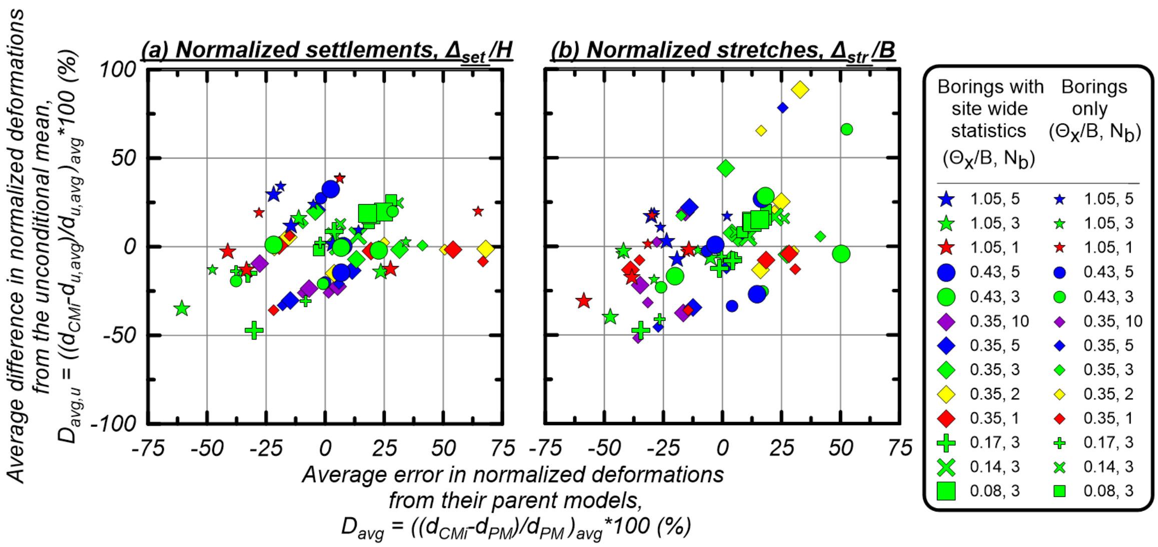


Figure 15: The average difference in normalized deformations relative to the mean for the unconditional models for sets of conditional analyses plotted against the average error in normalized deformations relative to the parent model for (a) normalized settlements and, (b) normalized stretches.